Proceedings of 20th IFAC Symposium on Automatic Control in Aerospace,
ACA 2016, 21 - 25 August 2016, Sherbrooke, Quebec, Canada.
In IFAC-PapersOnLine, Volume 49, Issue 17, 2016, pp. 320-325
DOI:10.1016/j.ifacol.2016.09.055

Design and Development of a Novel Spherical UAV

K. Malandrakis, **Roland Dixon**, **A. Savvaris** and **A. Tsourdos**

School of Aerospace, Transport and Manufacturing, Centre for Cyber-Physical Systems, Cranfield University, MK43 0AL, United Kingdom (e-mail: k.malandrakis@cranfield.ac.uk).

Abstract: This paper presents the design and system integration of a novel coaxial, flap actuated, spherical UAV for operations in complex environments, such as buildings, caves or tunnels. The spherical design protects the inner components of the vehicle and allows the UAV to roll along the floor if the environment permits. Furthermore, the UAV can land and take-off from any orientation and come into contact with objects without putting the propellers at risk. Flaps at the base of the sphere will generate roll and pitch moments as opposed to conventional swash plate designs while the coaxial setup will provide the necessary yaw moments and increase in thrust to volume ratio of the system. The flaps, placed below the propellers allow for decoupled roll and pitch control in a thrust vectoring manner. The final result of this design is a well-protected, compact, easily controlled, flexible and agile UAV for operations in complex environments. The spherical UAV was successfully flight tested on a number of occasions with various PD and μ-synthesis robust control systems and was observed to be easily stabilised and resistant to external disturbances to certain extent.

Keywords: Complex environments, spherical frame, robust control, μ-synthesis, contra rotating propellers, ultra-sonic sensor,test bench, coaxial rotor.

1. INTRODUCTION

1.1 Background

Over the past couple of decades the areas of applications of Unmanned Aerial Vehicle (UAV) have rapidly grown with platforms being tasked with increasingly more complex missions. More precisely, multi-rotors and small aerial vehicles have attracted considerable attention from the civil as well as military market because of their size, agility, cost of operation and ownership etc.

Nowadays, small aerial vehicles are used for example for surveillance and aerial monitoring, surveying and climate change research. Examples of the use of UAVs in commercial application are presented in Microdrones (2015), where quadrotors for industrial inspection, precision agriculture, surveying & mapping, remote sensing, and photogrammetric applications, were covered. Another example is given in Alpha (2015), where a small fire-fighting unmanned helicopter with an integrated Ground Control Station, is presented. Aeryon (2015) proposed quadrotor platforms for environmental sensing, private security, and tactical operations.

Indoor environments present other type of operational challenges such as restricted space for manoeuvring, GPS coverage, and the number of obstacles present in the operational environment. Several researchers have focused their research interest on fabricating smaller and more adaptive UAV designs to minimise the collision impact and increase the mission effectiveness in an indoor environment. However, another approach is to investigate and research the development of more innovative aerial vehicle designs and configurations. Parrot (2015) and Kalantari and Spenko (2013), presented two UAVs with similar design concepts that have a special frame, which allows the platform of performing both aerial and terrestrial locomotion in challenging terrains.

A spherical UAV, developed by the Japanese Defence Technical Research and Development Institute, was reported by Jonsson (2011). This vehicle is capable of flying in cramped and cluttered environments. There is no risk of propeller damage, since they are protected inside the structure.

1.2 Motivation

In this paper a spherical UAV, is proposed. The platform was designed to operate mainly in indoor complex environments such as buildings, caves, pipes, and sewerage systems. The design and size of the UAV was made, to be suitable for multiple operations such as monitoring & surveillance, pipeline inspection, mapping etc.

In order to navigate indoors, the aerial vehicle is equipped with ultrasonic sensors and an Inertial Measurement Unit (IMU). The spherical frame, which has an inner diameter of 22.6 cm, was developed in order to protect the propellers and the inner components in case the vehicle makes contact with a wall or a surface. Furthermore, the spherical design of the UAV allows the vehicle when the environment permits to roll along the ground. This could potentially be very useful for operations in very narrow spaces, for example, collapsed buildings following a disaster. Furthermore,

this could potentially also be a more energy efficient way to operate, hence increasing the operational endurance of the vehicle. Finally, the agility and manoeuvrability are guaranteed by the simulated model and control architecture of the system.

2. SYSTEM DESIGN AND STRUCTURE

The physical shape of the aerial vehicle, the choice of control actuators, the choice of hardware and electrical/electronic design are a vital step to ensure that the final aerial platform is one that is capable of supplying enough thrust to lift-off, enough control authority for stabilisation, enough computational power for control/sensor fusion and can supply the required voltage and current to all components at the same time. This section is subdivided into two main parts, namely: the mechanical design part; and the system integration part.

2.1 Mechanical Design

The light-weight and rigid mechanical structure of the system is shown in Fig. 1. It was designed such that it could provide maximum protection but also allow the aerial vehicle to manoeuvre freely and efficiently in a challenging environment. The compact size of the vehicle was achieved by the appropriate selection of components such as the ultra-nano-size servos and the 3-blade propellers. The most challenging part was the selection of the propulsion system.

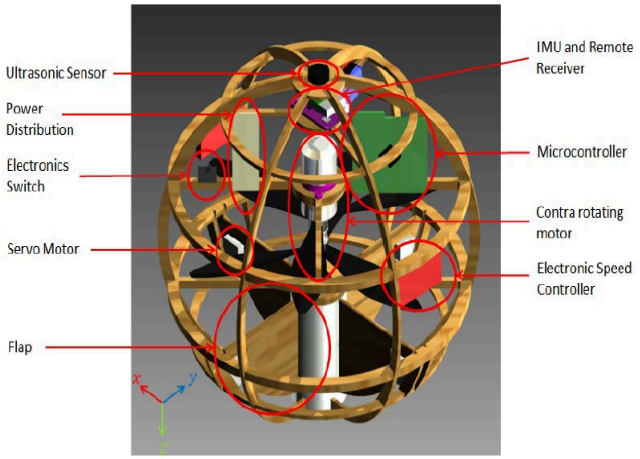

Fig. 1. CAD model of the spherical UAV showing the components' configuration in the vehicle.

According to references Koehl et al. (2012), Schafroth et al. (2010) and Bouabdallah et al. (2006) it was decided to select a contra-rotating motor. This type of motors could provide higher thrust, are compact, while having counter-rotating propellers cancel out the torque effect. The aerial vehicle light-weight structure was made from plywood. The material was used in the construction of the vehicles frame and flaps. The parts were designed in a 3D Computer-Aided Design (CAD) software and produced by a Computer Numerical Control (CNC) router. The total weight of the aerial vehicle is 0.59Kg.

It is worth mentioning that the key role of the four individually controlled flaps-surfaces, is to control the vehicle during flight. They have a 90^o separation around the inner circumference of the vehicle, and are located below the propellers along the vehicles x and y-axis. Therefore, a roll moment can be generated by constraining the flaps along the x-axis to move together whilst a pitch moment can be generated by constraining the flaps along the y-axis to move together. The yaw moment can be produced by the differential propeller speed.

2.2 System Integration

The hardware integration of the system, which is illustrated in Fig. 2, was proposed in order to provide sufficient attitude and altitude control of the vehicle. The hardware architecture is composed of an embedded system, sensors, communication modules, servos, and electronic speed controls (ESCs).

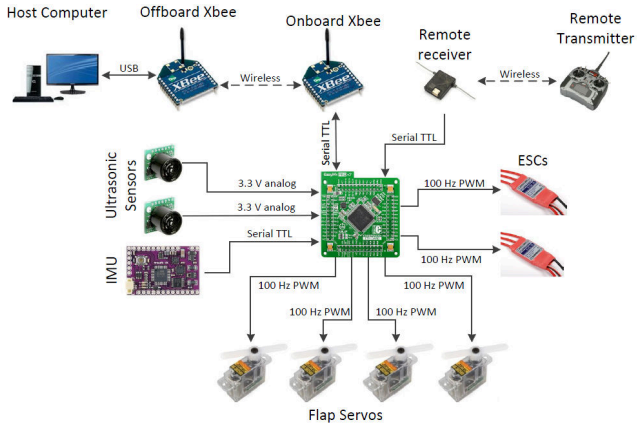

Fig. 2. Interconnections between the micro-controller and the hardware components on-board and off-board the UAV.

The micro-controller used on the spherical UAV is an STM32F407VG micro-controller made by ST Microelectronics. It runs at 168MHz and has 1MB of flash memory. It runs the control algorithms, for configuring flaps orientations and propellers angular velocity. The orientation of the flaps is regulated through the ultra-nano servos, while the propellers revolutions via the ESC-motor system. Each (18 Amps) ESC receives a PWM signal and supplies an individual motor of the contra rotating system with a three phase voltage. The micro-controller is connected with all the peripherals for receiving measurements or pilot commands and transmitting control signals to the control modules. Ultrasonic sensors are used to measure the distance to the ground and ceiling. The IMU provides attitude, acceleration and heading information. The IMU is running at a rate of 100 Hz, it consists of 3-axis gyroscope, 3-axis accelerometer and 3-axis magnetometer and it has a GPS port. A small and light receiver was selected that can accept direct pilot commands and feed them to the processing unit. Furthermore, the processing board has a bidirectional communication through an XBee module, operating at 2.4 GHz on the IEEE 802.15.4 physical radio specification, for real-time data acquisition. The Contra Rotating system, which consumes a maximum of 375 W, comprises two coaxial motors that are fixed with

two (8x4.5 inch three-blade) propellers. The maximum produced uninstalled thrust of the propulsion system is 13.1N that is sufficient to overcome the 5.78N weight of the platform. The spherical vehicle carries a 1300 mAh battery. There are two main power lines that come out of the battery, one going directly to the Electronic Speed Controllers (ESCs) and another going to the 3.3V power distribution board for all the electronic components. In its current configuration during normal operations, the UAV has an approximate flight time of around 10 minutes.

3. GROUND TESTING

A number of parameters are required in order to develop the mathematical model. Most of the data were obtained from series of experiments, the manufacturer data sheets and the CAD design.

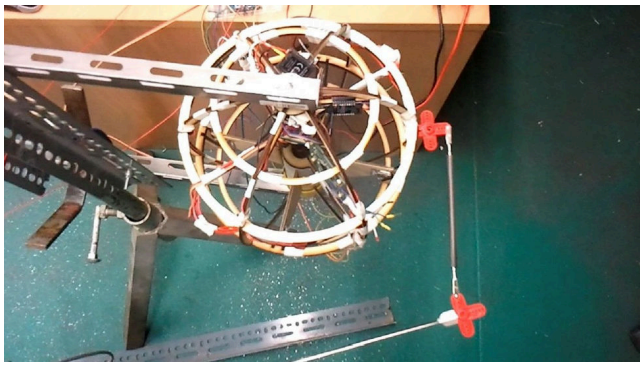

Fig. 3. Ground testing of vehicle on the test rig.

The ground testing of the vehicle was carried-out on a test rig for determining the thrust and torque coefficients by measuring the thrust and torque of the propulsion system. More precisely, the test rig was composed of rigid metallic parts and a strain gauge conductor, which is mounted on an especially designed flat beam. The strain gauge is an accurate sensor, however can be affected by several factors such as the temperature. For this reason, the strain gauge was calibrated prior to the testing to consider the temperature variation.

In Fig. 4 and Fig. 5, the overall generated thrust and torque, are presented, respectively.

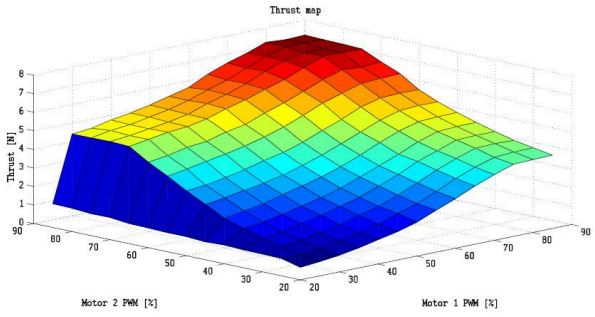

Fig. 4. Total produced thrust of the vehicle in function of two percentage throttle inputs. The vertical axis represents the total thrust in Newton while the horizontals the percentage throttle inputs for each motor.

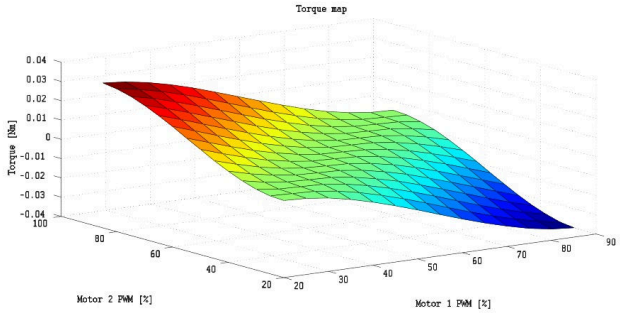

Fig. 5. Total produced torque of the vehicle in function of two percentage throttle inputs. The vertical axis represents the total torque in Newton meter while the horizontals the percentage throttle inputs for each motor.

It is worth mentioning that an essential amount of airflow is blocked by the components that restrict the overall productive thrust. According to the experimental data of the Fig. 4 and Fig. 5, the maximum generated installed thrust of the vehicle is 7.32 N, which correspond to around 44% of thrust loss, while the maximum torque is 0.027 N·m depending on rotation direction.

4. IMU SENSOR FUSION AND ALTITUDE LOCALISATION

The definition of the axes systems and their conversions, for each sensor, has a significant role in the IMU sensor fusion and the ultrasonic altitude localisation algorithms. More specifically, the IMU consists of an MPU-6000 system, which provides rotational rates and acceleration data, and a magnetometer, which measures magnetic field data.The coordinate system of MPU-6000 is left-handed while in the magnetometer,which is located on the underside of the IMU, is right-handed. Therefore, the axis system of each sensor was orientated in a way that the Extended Kalman Filter (EKF) can generate successfully the angles of the body axis of the spherical vehicle. A transformation matrix in quaternion form is implemented to convert the Earth axis system into the autonomous vehicle (body) axis system.

The sensor calibration is critical step to ensure that the effect of sensor bias and scaling errors do not affect the integrity of the final sensor reading, especially with rate or relative sensors that require measurements integration at every step that will accumulate the sensor inaccuracies.Therefore, during the experiments, a sequence of sensor calibrations was carried-out.

4.1 IMU Sensor fusion

The recorded IMU body rates , the acceleration vector and the magnetometer vector are fused by a quaternion based EKF to acquire corrected, drift-free Euler angles updates from the IMU, at every time step. The quaternions have the advantage of being more computationally efficient and effective than the Euler angles because of the avoidance of singularities and computationally complex functions.

In Fig. 6 the flowchart of the IMU Kalman Filter with the roll and pitch updates from the accelerometer and

the yaw update from the magnetometer, is presented. The two measurement update phase has the advantage that the magnetometer update phase can be excepted from the Kalman Filter in circumstances with high magnetic interference. Hence, only the pitch and roll will be updated at each time step.

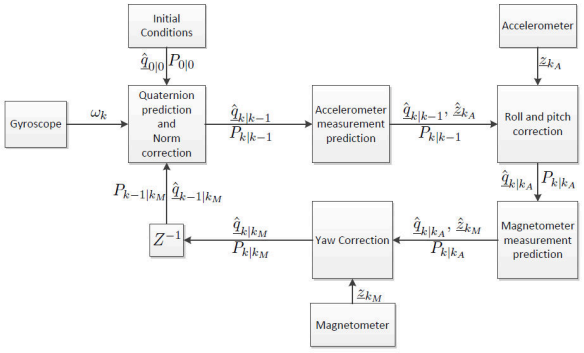

Fig. 6. Flowchart of IMU EKF.

The system update in discrete time and in quaternion form, is given as

$$q_k = (I + AT)q_{k-1} + w_k = \Phi_k q_{k-1} + w_k$$

where q_k defines the quaternion vector at time step k and w_k the acting noise on the system, that is presumed to be Gaussian distributed with zero mean noise. Thus, the system update equation for the Extended Kalman Filter is expressed as,

$$\hat{q}_{k|k-1} = \Phi_k \hat{q}_{k-1|k-1_M}$$

where $\hat{q}_{k|k-1}$ is the prior estimated mean of the quaternion vector at time step k taking into consideration the posterior estimated mean from the magnetometer one time step before $\hat{q}_{k-1|k-1_M}$. The system update is known as the prior belief of the system about its state before measurement update and is represented by a multi-modal Gaussian/normal distribution with mean $\hat{q}_{k|k-1}$ and covariance $P_{k-1|k-1}$

When the spherical UAV was tested, with the IMU mounted, the motors were generating high magnetic interferences. As a result, the yaw was updated according to the magnetic north of the motors instead of the magnetic north of the Earth. For this reason the yaw update from the EKF, was neglected. The effect of the yaw drift is not as considerable as the effect of the pitch and roll drift because it will not cause instability in flight unless it is very fast and the spherical UAV will not control yaw directly but rather control the yaw rate and therefore does not require an accurate yaw measurement. The results of the sensor fusion algorithms with the magnetometer and without the magnetometer, were generated from real recorded data. The IMU sensor fusion algorithm was shown to be robust even when extra, simulated, noise was added and proved reliable, drift free, measurements for use in the control systems.

4.2 Ultrasonic Altitude Localisation

The ultrasonic localisation was intended to be used for altitude updates and control. The ultrasonic sensors were placed at the bottom and the top of the spherical UAV so that measurements could be taken from the floor and roof, for additional robustness in the algorithm. Therefore, the primary aim of this algorithm was to correct the Earth axis velocity and down position based on range measurements, in indoor environments, produced by the altitude sensors.

In the algorithm of EKF, a measurement validation step, was added to ensure that false readings made by the ultrasonic sensors are not incorporated with the altitude measurement update, as is presented in Fig. 7.

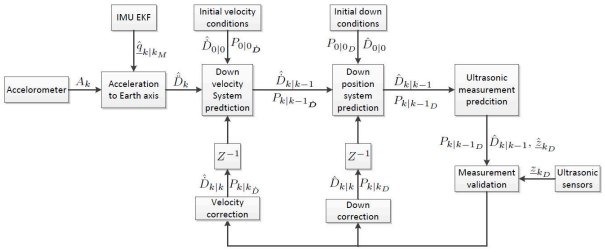

Fig. 7. Flowchart of ultrasonic Kalman Filter.

At this flow diagram, the down position of the IMU, is defined with D at time step k.

According to the experimental process, the algorithm gave satisfactorily results when the motor were off. However, when the motors were turned on, the produced acoustic noise, the air turbulence from the propulsion system and the unstable power supply, which is caused by the current draw from the motors, had a major affect on the sensor measurements. For this reason, both ultrasonic modules and the localisation for altitude control were not applied in real-time for feedback to the control system of the spherical UAV. Hence, in the future the ultrasonic sensors will be replaced by two light-weight lidar units.

5. CONTROL DESIGN

The design of spherical UAV allowed for decoupling of the lateral, longitudinal and the vertical dynamics. Flaps along the body x-axis were constrained to move together, thereby controlling the lateral dynamics (namely roll) and the flaps along the body y-axis were constrained to move together, thereby controlling the longitudinal dynamics (namely pitch). The vertical dynamics of the spherical UAV was composed of the thrust along the body z-axis and the torque about the body z-axis, both generated by the coaxial motor-propeller sets. Thrust and torque tests about the body z-axis were carried out to obtain mappings between the input PWM to motor drivers and the thrust and torque produced. In this way the vertical dynamics of the spherical UAV could be modelled with minimum uncertainty. The lateral and longitudinal dynamics were modelled based on pure theory and the mass properties obtained from a 3D CAD drawing and therefore had an amount of uncertainty. Non-linear, rigid body dynamics were used for the spherical UAV and control algorithms were designed about the hovering trim state of the sphere that introduces even more uncertainty. For these reasons, a Proportional Differential (PD) controller was designed for the vertical dynamics and a robust controller, that takes

uncertainty into consideration, was initially designed for the lateral-longitudinal dynamics. Ultrasonic sensors were fitted to the initial design of the sphere to obtain appropriate Earth axis down positions, it was quickly ascertained that the acoustic noise generated by the propellers provided far too much interference for the ultrasonic distance measurements to be reliable and therefore altitude of the spherical UAV was controlled directly through pilot intervention.

Fig. 8 shows the structure of the control system for the vertical dynamics. The body axis yaw rate (r) is controlled by two PD controllers (one for each motor).

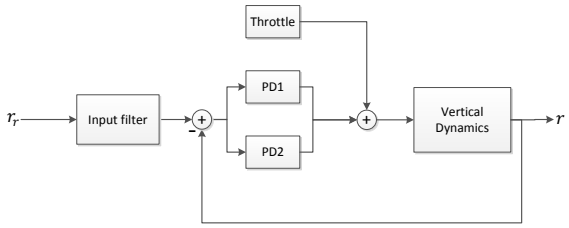

Fig. 8. Vertical Control System.

Fig. 9 shows the robust control system design for the lateral-longitudinal dynamics where K_{xy} is the robust control system and G_{xy} is the lateral-longitudinal dynamics of the sphere. The μ-synthesis technique was used with the MATLAB® Robust Control Toolbox. The design procedure was a model matching one with $W_{Q_{xy}}$ being the goal, second order dynamics of the sphere. Frequency weighting $W_{B_{xy}}$ was used to tune model matching characteristics over specific frequency regions, $W_{A_{xy}}$ was used to press down on flap actuation to avoid saturation over certain frequency regions, $W_{u_{xy}}$ and Δ_{xy} are used to model the uncertain longitudinal-lateral dynamics. $W_{N_{xy}}$ is used as a noise generator so that the design control system can account for high frequency noise in the system and sensor dynamics.

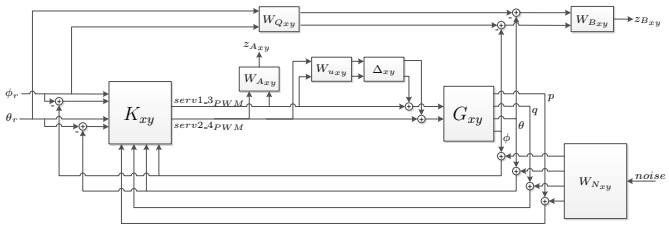

Fig. 9. Lateral-longitudinal control system design.

Fig. 10 shows the results of the lateral-longitudinal robust control system. It can be seen that the spherical UAV is not very responsive to control inputs, it is very stable in flight (it does not move off its hover point very easily) and it has a slight negative roll attitude at hover. From the robust controller results it was ascertained that the non-linear model did not take an unknown source moment into consideration that was restoring the sphere to hover position during flight. The complexity of the robust controller did not allow for a huge amount of insight into the

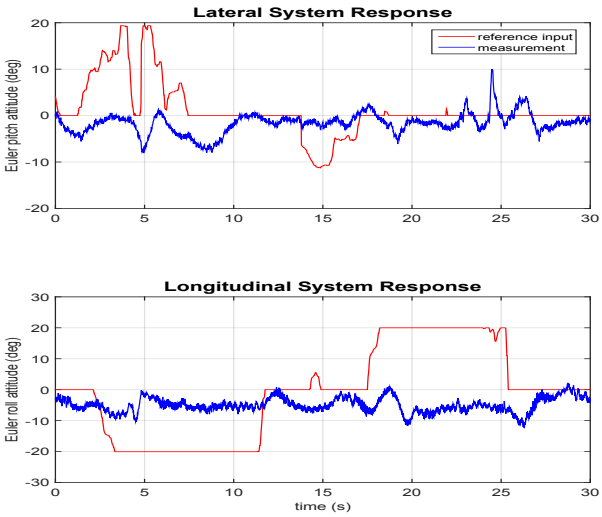

Fig. 10. Lateral-longitudinal control with robust control system.

system and did not allow for tuning. Two solutions were proposed now that it was known what type of response was needed to stabilise the lateral-longitudinal dynamics. The first design solution was to alleviate the effects of the restoring moment by changing the centre of gravity of the sphere and then use individual PD controllers for the lateral and longitudinal dynamics, this would allow for insight into the system and tuning of the controller gains. The second solution was to include an integral gain to the control system as to overcome the restoring moment, this has the disadvantage of actuator saturation. The former solution was chosen.

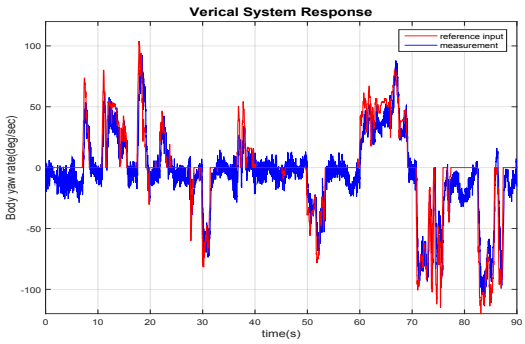

Fig. 11. Vertical PD control system.

Fig. 11 shows the results of the PD controllers about the vertical axis. The body yaw rate response to a differential propeller speed is of type 1 (has a pole at the origin) and therefore a PD controller is adequate to ensure zero steady state error as seen in the figure.

Fig. 12 shows the PD structure of the lateral-longitudinal dynamics. Inner loop controller K_p and K_q control the roll and pitch rate, respectively, whilst the outer loop controllers K_ϕ and K_θ controlled the roll and pitch perturbed Euler attitudes, respectively.

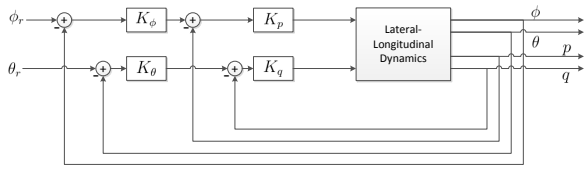

Fig. 12. Lateral-longitudinal PD control structure.

Fig. 13 shows the results of the lateral and longitudinal PD control systems. In this point is worth noting, that also an integrator was tested but was fast rejected because it forced actuator saturation too quickly,during the experimental process. Furthermore, based on the control theory of this system, there is no need for I controller in the rotational dynamics.

It can be seen that the inner loop dynamics are not type 1 as expected from the linearised model so a restoring moment was still present even under the influence of substantial weighting. The response to reference inputs was seen to be a lot better than the robust control system after substantial control system tuning. The spherical UAV can still be seen to have slight negative roll attitude which has the effect of causing flap saturation when trying to achieve a positive roll.

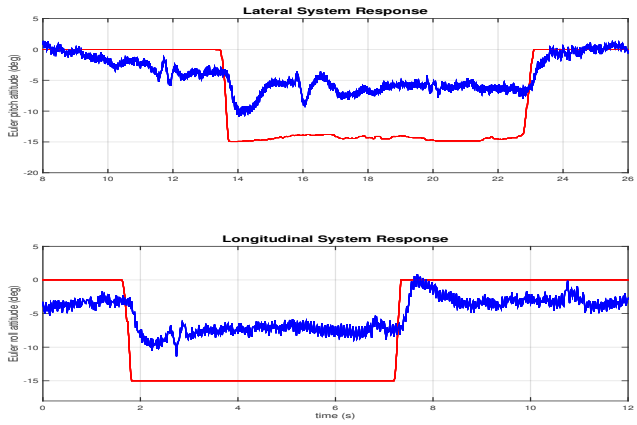

Fig. 13. Lateral-longitudinal PD control results.

The presented steady-state error of Fig. 13 is due to the lack of integral control and the inadequate actuation authority. A way to enhance the authority of actuators (flap) is to be shifted further down from the CG and be replaced by more efficient aerofoil designs in order to produce adequate moments.

6. CONCLUSIONS

A new spherical UAV was designed, built and flight tested. It was found to be very stable in flight and did not achieve zero steady state error for the lateral and longitudinal dynamics under the influence of both the robust control system and the PD control system. This reason for not achieving zero steady state error is caused by a moment that attempts to restore the spherical UAV to hovering trim state and therefore roll and pitch rate dynamics are not type 1 and therefore integral action will be needed by the controller. Shifting centre of gravity, the restoring effect was reduced a little but was still present. The vertical dynamics of the spherical UAV achieved good steady state error and responded quickly to changes in the reference input.

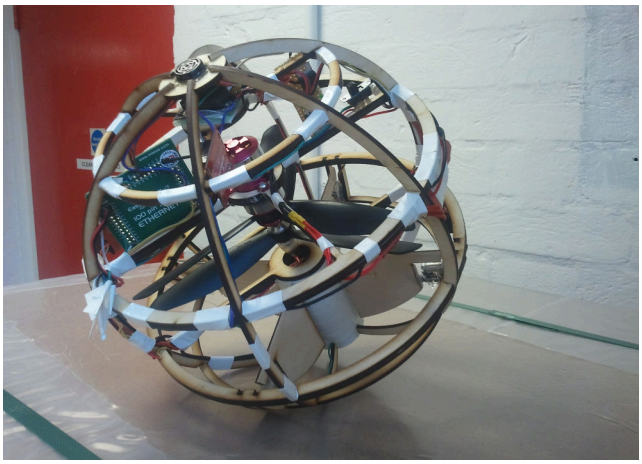

Fig. 14. The completed flight ready spherical UAV.

REFERENCES

Aeryon (2015). Aeryon small Unmanned Aerial Systems (sUAS) Aeryon Labs Inc. URL `http://aeryon.com/`.

Alpha (2015). Home | Alpha - Unmanned System. URL `http://www.alphaunmannedsystems.com/`.

Bouabdallah, S., Siegwart, R., and Caprari, G. (2006). Design and control of an indoor coaxial helicopter. In *Intelligent Robots and Systems, 2006 IEEE/RSJ International Conference on*, 2930–2935. doi:10.1109/IROS.2006.282146.

Jonsson, R. (2011). Japanese defense ministry shows world's first spherical flying machine. URL `http://www.gizmag.com/japanese-spherical-flying-machine/20286/`.

Kalantari, A. and Spenko, M. (2013). Design and experimental validation of HyTAQ, a hybrid terrestrial and aerial quadrotor. In *Robotics and Automation (ICRA), 2013 IEEE International Conference on*, 4445–4450. IEEE.

Koehl, A., Rafaralahy, H., Boutayeb, M., and Martinez, B. (2012). Aerodynamic modelling and experimental identification of a coaxial-rotor uav. *J. Intell. Robotics Syst.*, 68(1), 53–68. doi:10.1007/s10846-012-9665-x. URL `http://dx.doi.org/10.1007/s10846-012-9665-x`.

Microdrones (2015). UAV / drone solutions for mapping, aerial inspection, unmanned cargo. URL `https://www.microdrones.com/en/home/`.

Parrot (2015). Parrot Minidrones Rolling Spider, Fly and roll anywhere. URL `http://www.parrot.com/products/rolling-spider/`.

Schafroth, D., Bermes, C., Bouabdallah, S., and Siegwart, R. (2010). Modeling and system identification of the mufly micro helicopter. *J. Intell. Robotics Syst.*, 57(1-4), 27–47. doi:10.1007/s10846-009-9379-x. URL `http://dx.doi.org/10.1007/s10846-009-9379-x`.